Composites: Part B 43 (2012) 2676–2686

Contents lists available at SciVerse ScienceDirect

Composites: Part B

journal homepage: www.elsevier.com/locate/compositesb

Monitoring mechanical damage in structural materials using complimentary NDE techniques based on thermography and acoustic emission

E.Z. Kordatos, D.G. Aggelis, T.E. Matikas *

Department of Materials Science and Engineering, University of Ioannina, 45110 Ioannina, Greece

ARTICLE INFO

Article history:
Received 15 October 2011
Received in revised form 20 December 2011
Accepted 31 December 2011
Available online 10 January 2012

Keywords:
A. Metal–matrix composites (MMCs)
B. Fracture
IR thermography
D. Non-destructive testing
D. Acoustic emission

ABSTRACT

This work deals with nondestructive evaluation (NDE) of the fracture behavior of metallic materials by combining thermographic and acoustic emission (AE) characterization. A new procedure, based on lock-in infrared (IR) thermography, was developed to determine the crack growth rate using thermographic mapping of the material undergoing fatigue. The thermography results on crack growth rate were found to be in agreement with measurements obtained by the conventional compliance method. Furthermore, acoustic emission was used to record different cracking events. The rate of incoming signals, as well as qualitative features based on the waveform shape, was correlated with macroscopically measured mechanical parameters, such as load and crack propagation rate. Additionally, since the failure modes have distinct AE signatures, the dominant active fracture mode was identified in real time. The application of combined NDE techniques is discussed for characterizing the damage process which leads to catastrophic failure of the material, thereby enabling life prediction in both monolithic aluminum alloys and aluminum alloy/SiC particle (SiC_p) reinforced composites.

1. Introduction

Infrared thermography is a powerful nondestructive evaluation tool which can be effectively used for defect detection in materials such as aluminum alloys and metal matrix composites. Aluminum alloys exhibit good resistance to corrosion, as well as high strength in operational conditions at high temperatures. Silicon carbide particulate-reinforced aluminum matrix composites possess improved physical and mechanical bulk properties compared to wrought matrix alloys. The use of SiC_p reinforced aluminum matrix composites as a substitute for monolithic aluminum alloys in structural applications, especially in the aerospace and automobile industry, is becoming increasingly attractive [1]. In the aerospace industry, where inspection is of paramount importance in all fabrication stages, there is a need for fast, reliable nondestructive assessment techniques. Infrared lock-in thermography can fulfill this need because it is a quick, full-field and real-time inspection tool, which can be used to examine a relatively large area of a structure and aircraft components [2,3]. It is also a noncontact technique; the equipment is fairly portable and hence can be used reasonably easily in the field [4].

Lock-in thermography provides a powerful tool to study thermo-mechanical mechanisms. Instead of a simple temperature rise measurement, which depends on environmental conditions, lock-in thermography locates and measures thermal sources, which are proportional to thermo-mechanical energy, under harmonic loading and adiabatic conditions [5]. This method is based on the direct correlation between thermal variations, caused by thermal excitation due to mechanical fatigue, and thermal stresses established by applying thermo-elasticity principles [6,7]. Furthermore, quantitative infrared thermography as a nondestructive and noncontact technique has been used to detect manifestation of the physical process of fatigue and to evaluate rapidly the fatigue limit of materials or mechanical components [5,8–10].

A major advantage of IR thermography applications is the detection and monitoring of sub-surface cracking. Optical IR thermography has been used for the measurement of crack length in compact tension specimens in order to calculate the stress intensity factor (ΔK) [11]. In addition, it has been employed for detection of cracks due to local temperature increment, determination of crack initiation and prediction of crack propagation [12]. Moreover, this method has been used for crack growth monitoring of single edge notch tension specimens during fatigue testing [13]. Thermography has also been used for evaluating the state of damage in materials undergoing cyclic mechanical loading by analyzing thermal effects in these materials caused by fatigue [14,15].

In the present study, acoustic emission (AE) was complementarily used for monitoring fracture behavior of metal coupons. Acoustic emission is widely used for structural health monitoring of a variety of materials and structures. After the landmark work of Kaiser [16] more than 60 years ago, AE has been extensively

* Corresponding author.
E-mail address: matikas@otenet.gr (T.E. Matikas).

1359-8368/$ - see front matter © 2012 Elsevier Ltd. All rights reserved.
doi:10.1016/j.compositesb.2011.12.013

used for inspection of metals and other materials. It makes use of the energy that is released from crack nucleation and propagation in the form of elastic waves. This energy propagates through the material and is detected by piezoelectric sensors mounted on the surface of the material [17]. The cumulative AE activity depends on the severity of cracking, since crack propagation is the source of the emissions. High rate of recorded signals indicates the existence of numerous active cracks. On the other hand, low activity denotes intact conditions. When multiple sensors are applied, the location of cracks can be calculated from the arrival of waves at the measurement positions at different time instances [18]. Apart from the total acoustic activity other important features of AE data enlighten different aspects of the fracture process, such us the damage mode. The AE waveform shape depends on motion of the crack tip and carries information on cracking mode. Generally, tensile cracks precede as the material is being fractured. Therefore, crack characterization may lead to an early warning. In the event of a tensile cracking occurrence, the crack faces move away from each other. This results in a transient volumetric change in the vicinity of the crack and transmits most of the energy is in the form of longitudinal waves. Since longitudinal waves are the fastest, most of the released energy is recorded quite early within the waveform. Fig. 1 shows examples of AE waveforms originating from tensile and shear events. For the tensile event, the delay between the onset and the highest peak (called rise time, RT), is short leading to a high rise angle of the wave. In the event of a shear crack, the shape of the vicinity near the crack is transiently affected, shifting the proportion of energy to shear waves, which are slower. Therefore, the most important part of the waveform arrives later than the fast longitudinal arrivals, leading to longer RT and consequently small rise angle (see right of Fig. 1). In plate geometries, a direct correspondence exists with vertical matrix cracking resulting in strong symmetric modes, while parallel cracks/delaminations shift the proportion in favor of the anti-symmetric ones [19]. Recently the shape of the initial part of the waveform is quantified by the RA value which is defined as the RT over the Amplitude, A, and is measured in μs/V (or ms/V), as suggested by relevant recommendations [20]. Additionally, tensile events carry higher frequency content. A rough but valuable expression of the frequency content is the average frequency (AF) defined by the number of threshold crossing (simply counts in AE terminology) over the signal duration [21]. The "threshold" is a user-defined voltage in order to avoid environmental or other noise, but at the same time should be sensitive enough to allow acquisition of the AE hits related to crack propagation.

Classification of AE waveforms based on the RA and AF has proven quite successful in a number of laboratory applications concerning concrete cracking [21,22], fracture of composite laminates [23,24], as well as the discrimination between matrix cracking and pull out during bending of fiber reinforced concrete [25]. In studies related to metal and composite plates, AE amplitude has been correlated to stress in fracture of composite metal foam specimens [26] and composite sandwich panels [27]. Cumulative AE energy has been correlated to temperature profile of composites under fatigue [28]. Furthermore, the cumulative AE activity has been related to strength and the number of breaks in fiber fragmentation tests [29,30], as well as to the remaining life in fatigue tests of steel specimens with notches [31]. Concerning aluminum matrix materials, AE parameters such as rise time and duration have been considered in an attempt to correlate with corrosive processes [32]. In these studies, several AE features, such as peak frequency, central frequency, rise time, amplitude and energy have been correlated with irreversible processes in the material, such as oxide formation or hydrogen evolution. In other studies, AE signals have been used in fiber fragmentation tests to record the number of breaks and their location [33]. Parameters like rise time, duration and RA have shown strong sensitivity to the crack propagation rate and were used to characterize the transition from tension to shear failure in compact tension specimens under fatigue [34].

In this study, aluminum compact tension coupons and A359/SiC_p composite specimens were subjected to tension–tension fatigue until fracture. During the tests the accumulated damage was monitored concurrently with lock-in thermography and acoustic emission. A novel nondestructive methodology, based on lock-in thermography, was developed for determining crack growth rate in specimens undergoing fatigue. This new method was also applied for investigating the influence of heat treatment processing conditions on fracture properties of the material. Acoustic emission activity was also monitored to check for possible transition of AE features as the crack propagation rate increases and damage is being accumulated. Waveform parameters that have been shown sensitive to damage mode in different materials were examined for their efficiency in damage monitoring in terms of crack propagation rate and transition between successive modes.

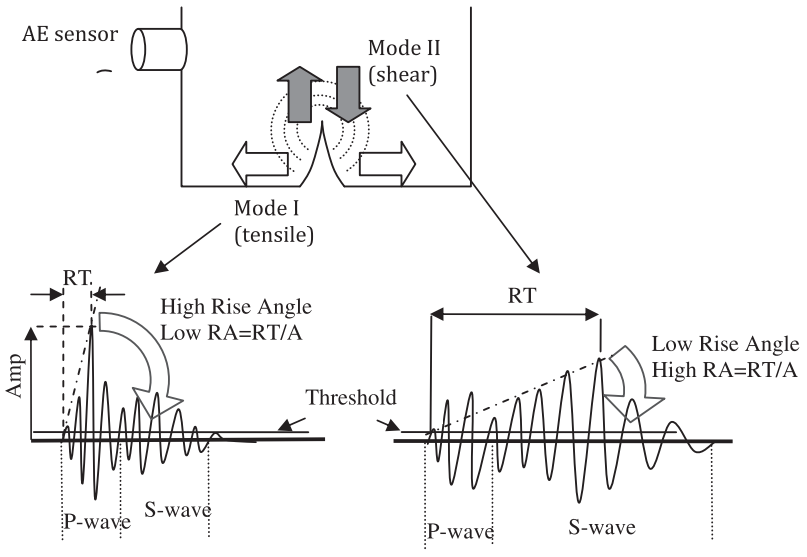

Fig. 1. Cracking modes and corresponding AE signals.

2. Theoretical background of lock-in thermography

In this paper, fatigue crack propagation was monitored using infrared thermography and crack-tip stress field was mapped using thermo-elasticity principles. The technique is based on the fact that when a solid material is rapidly stressed by external or internal loads and adiabatically deformed, the phenomenon is accompanied by simultaneous variation of temperature. When the material is under tensile loading, its temperature decreases proportionally to the load, however, when it is under a compressive load its temperature increases proportionally to the load. This behavior is known as the thermo-elastic effect.

The thermo-elastic effect refers to the thermodynamic relationship between the change of stress in a component under elastic loading and the corresponding change of temperature. It is simply proportional to the change in the sum of principal stresses, if adiabatic conditions prevail. Combining the first and second principles of thermodynamics the local heat changes can be described by Eq. (1).

$$\rho C T - k\nabla^2 T = r + s_{\text{the}} + d_1 \tag{1}$$

In Eq. (1) ρ represents the mass density, C is the specific heat (at constant pressure) and k is the conduction. The different heat sources are cumulated in the terms of external source supply "r", of thermoelastic source "s_{the}" and of intrinsic dissipation "d_1". To simplify Eq. (1), the followings hypotheses are required: (a) mass density and specific heat are material constant, (b) convective term is negligible because of velocity amplitude is very small, (c) the material is isotropic from the heat conduction point of view and (d) external sources are time independent and give the equilibrium temperature of the specimen (T_0). So, the simplified heat diffusion equation is:

$$\rho C \Theta - k\nabla^2 \Theta = s_{\text{the}} + d_1 \tag{2}$$

where $\Theta = T - T_0$ is the temperature variation.

To simplify Eq. (2) it could be considered that the rate of temperature change (Θ) is much larger than the Laplacian term ($\nabla^2\Theta$). That condition is usually expressed in term of minimum frequency to assure that the equation can be written as:

$$\rho C \Theta = s_{\text{the}} + d_1 \tag{3}$$

For low level of stress, the dissipated energy is negligible compared to the thermo elastic production of heat. So the Eq. (3) is simplified to:

$$\rho C \Theta = s_{\text{the}} \tag{4}$$

For linear isotopic material, under plane stresses, the thermo-elastic energy can be written as:

$$s_{\text{the}} = -\alpha T_0 \sigma \tag{5}$$

where σ is the sum of principal stresses. Finally, Eqs. (4) and (5) lead to the equation of thermo-elasticity described by Thomson [35]:

$$\rho C \Theta = -\alpha T_0 \sigma \tag{6}$$

Eq. (6) is valid for linear isotropic, homogeneous material if adiabatic conditions prevail. The change of temperature is proportional to the change of the sum of the principal stresses.

Moreover under sine loading the above relationship between temperature and the sum of principal stress is valid for the peak to peak value (Eq. (7)).

$$\Delta\Theta = -\frac{\alpha}{\rho C}\Delta\sigma = K_m T_0 \Delta\sigma \tag{7}$$

In Eq. (7) K_m is the thermo-elastic coefficient. [36]

An experimental setup can be used to map the distribution of the sum of principal stresses in the structure [5]. This setup includes a radiometric camera, which measures the infrared radiation produced on the surface of the material undergoing cyclic loading, and a real-time correlator called "lock-in module", which measures the slight change of temperature extracting it from the noise that is specified by thermal resolution of the camera. Lock-in refers to the necessity to monitor the exact time-dependence between the output signal and the reference input signal [37]. This is done using a lock-in amplifier so that both phase and magnitude images become available.

The principle of lock-in thermography (Fig 2) is based on the synchronization of the camera with the source of heating, which can be optical excitation, ultrasound, cyclic loading of the material, etc. In the case that a specimen undergoes cyclic loading, heat waves are generated and the resulting oscillating temperature field in the stationary regime is recorded remotely through thermal infrared emission. The frequency of modulation varies with the nature, size and shape of defects to be detected. Using this method, the influence of emissivity and non-uniform heating on the temperature measurement is reduced allowing inspection of large areas of samples with high repeatability and sensitivity [38,39].

3. Experimental procedure

This section presents information on the materials tested, the testing conditions as well as the experimental NDE procedures used for monitoring damage on-site, during the tests.

3.1. Materials and mechanical testing

The materials used in this research were aluminum (AA 7075) and hot rolled A359 aluminum alloy reinforced with 31% SiC. Two different heat treatments were applied on the A359/SiCp samples; T6 and HT-1. The "as received" condition is referred as T1 condition. In the solution heat treatment T6 the material was heated to a temperature below the initial melting point of the alloy for 2 h at 530 ± 5 °C. Thus, all the solute atoms were allowed to dissolve to form a single-phase solid solution before being quenched in water. Next, the composites were heated to a temperature of 155 °C for 5 h and subsequently cooled in air. In the solution heat treatment HT-1 the material was heated to a temperature lower than the T6 condition that is 450 ± 5 °C for 1 h, and then quenched in water. Subsequently, the alloy was heated to an intermediate temperature of 170 °C for 24 h in the age hardened stage and then cooled in air [38,39]. This study mainly intends to present the monitoring of fracture behavior in real time during the tests.

The chemical compositions of the materials at the as received state are presented in Tables 1 and 2. Test specimens were manufactured according to ASTM E399-09e1 [38]. The geometry of the specimens is shown in Fig. 3.

For the determination of crack propagation rate (CPR), a crack opening displacement (COD) meter was fixed at the notch opening. The determination of crack propagation rate followed ASTM E647-08e1 standard [39]. The fatigue tests were conducted using an INSTRON servo-hydraulic machine with maximum dynamic load range of ±100 kN. The fatigue cycle was sinusoidal with a frequency of 3 Hz, stress ratio $R = 0.2$, and amplitude of 4 kN.

3.2. Lock-in thermography method

Lock-in IR thermography was used for non-contact monitoring of crack propagation during the test. This newly developed methodology, based on thermographic assessment of fracture, enabled determination of crack growth rate. For this reason, an infrared

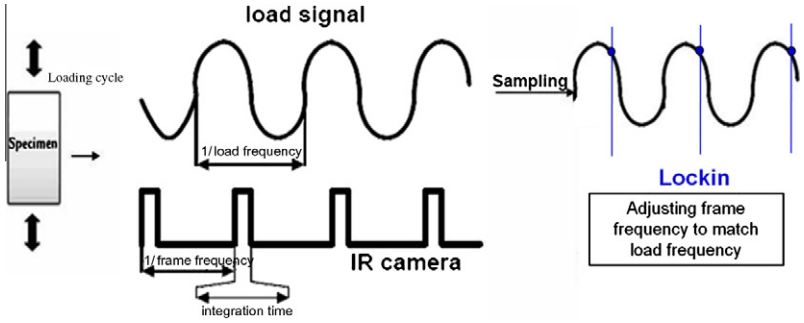

Fig. 2. Lock-in thermography principle.

Table 1
Chemical composition of AA 7075.

Material	Elements (wt.%)							
AA 7075 En 573-3 (AlZnMgCu1,5F53)	Cu	Si	Zn	Pb	Fe	Mg	Mn	Ti
	1.20 – 2.00	Max 0.40	5.10 – 6.10	1.00 – 2.50	Max 0.50	2.10 – 2.90	Max 0.30	Max 0.20

Table 2
Chemical composition of the silicon carbide particulate-reinforced A359 aluminum alloy matrix composite.

Material	Elements (wt.%)					
A359/SiCP (31%)	Si	Mg	Mn	Cu	Fe	Zn
	9.50	0.50	0.10	0.20	0.20	0.10

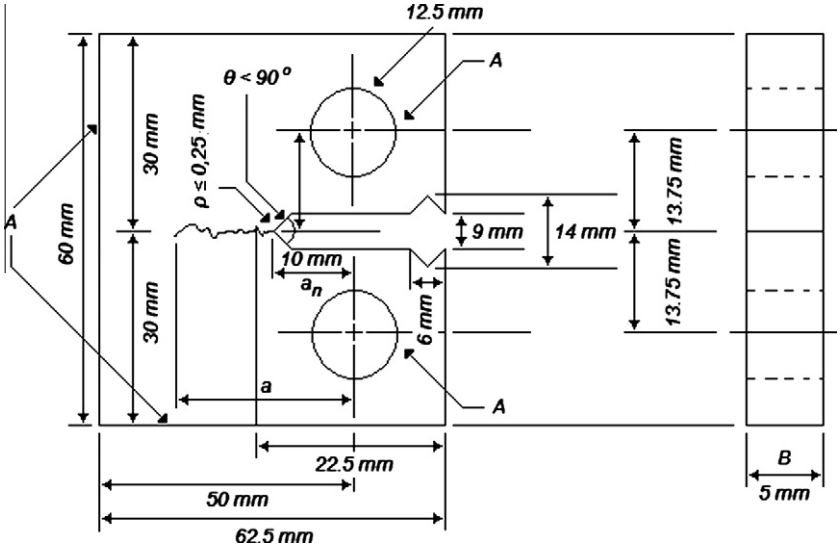

Fig. 3. Specimen geometry.

camera was placed at a distance from the specimen. The IR camera was connected with the lock-in amplifier and the amplifier with the main servo-hydraulic controller. Therefore, synchronization of the frequency through the lock-in amplifier and the testing machine could be achieved and lock-in images and data capture during fatigue testing were enabled (Fig. 4). The experiments were conducted using an infrared camera CEDIP (MIW) with a cooled indium antimonide (InSb) detector (3–5 μm), a frame rate of 150 Hz and a focal plane array (FPA) with pixel format of 320 (H) × 240 (V). The resolution of the IR camera was 20 mK and the integration time is 1500 μs.

In order to determine the crack growth rate using thermographic mapping of the material undergoing fatigue a specific procedure was developed. This procedure consists of the following steps: (a) the distribution of temperature and stress on the surface of the specimen was monitored during fatigue testing using lock-in thermography. (b) Thermal images were saved as a function of testing time in the form of a movie for post-processing. (c) After the test was concluded, in post-processing mode, equally spaced reference lines were set on the thermographic image in front of the crack-starting notch (Fig. 5a and b). (d) Along these lines the stresses were estimated using the thermographic data for a specific

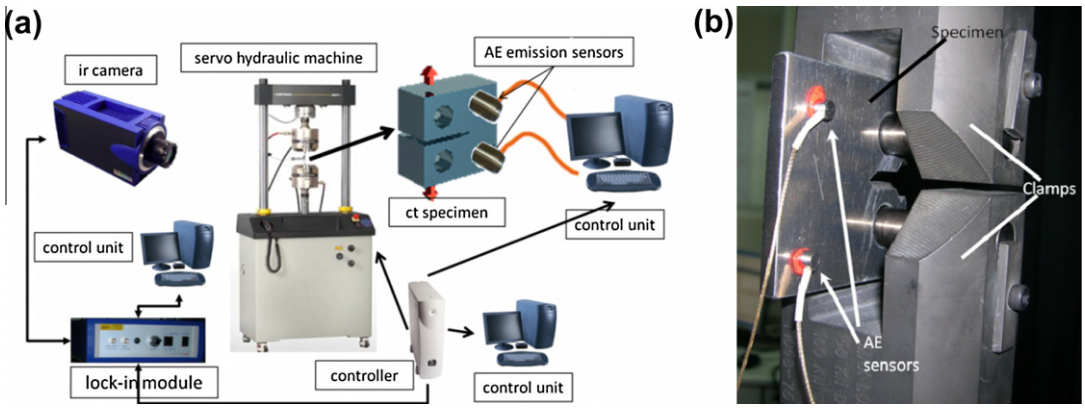

Fig. 4. Experimental setup.

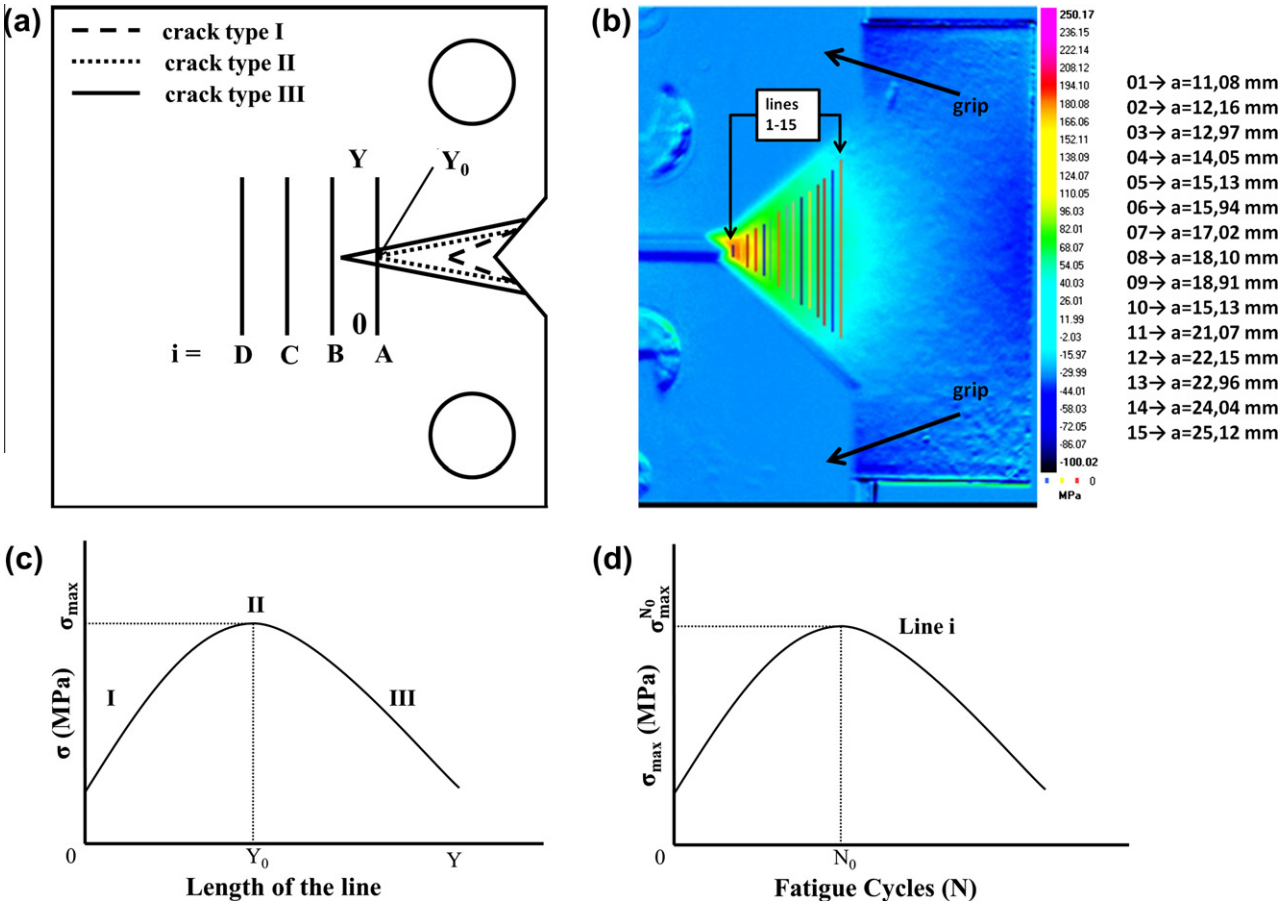

Fig. 5. Lock-in thermography method: (a) schematic of CT specimen showing 4 lines vertical to the crack propagation direction, (b) thermal image with equally spaced reference lines, (c) schematic of stress estimation along a particular reference line for a specific cycle, and (d) schematic of maximum stress along a particular reference line vs. number of fatigue cycles.

fatigue cycle. The idea was based on the fact that the stress monitored at a specific location vs. time (or fatigue cycles) would increase when the crack approaches the line (crack type I), then would attain a maximum value when the crack tip reaches that reference line at the point Y_o (crack type II), and finally would decrease when the crack has crossed that line (crack type III), as it is shown in Fig. 5a and c. (e) The stress was also monitored during the test for all fatigue cycles. Fig. 5d shows the maximum values of stress along a specific reference line vs. the number of fatigue cycles. The cycle N_o for which this stress maximum occurs denotes the moment that the crack crosses that reference line.

3.3. Acoustic emission testing

The acoustic emission monitoring was conducted using two piezoelectric sensors (Pico, Physical Acoustics Corp., PAC) mounted on one side of the specimen (see Fig. 4b). The sensors were attached using electron wax, which supported the sensors during the experiment, while supplying the necessary acoustic coupling. These sensors are considered broadband with frequency bandwidth between 50 and 800 kHz and maximum sensitivity at 450 kHz. The AE signals were recorded by two channels in a PCI-2 board, PAC with a sampling rate of 5 MHz. The acquisition

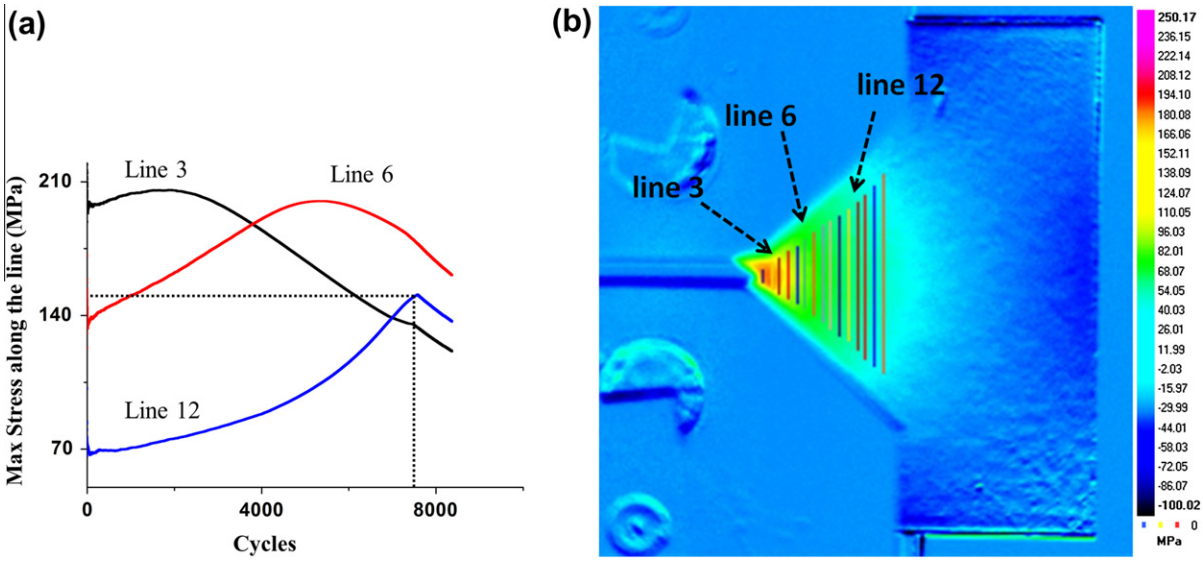

Fig. 6. (a) Diagram of max stress along 3 typical reference lines vs. fatigue cycles, and (b) thermograph of 3 plotted reference lines.

threshold was set to 40 dB to avoid recording ambient noise, while the acquired signals were preamplified by 40 dB.

4. Lock-in thermography results

The aforementioned method for thermographic monitoring was applied to five AA7075 specimens and five specimens for each different heat treatment conditions (T1, T6, HT1) of A359/SiCP (31%). Using the procedure described in Section 2, the local stress vs. time (cycles) was measured along each of the fifteen reference lines placed in front of the notch.

Fig. 6a illustrates the maximum value of stress vs. the number of fatigue cycles for three different typical lines (Fig 6b) of the fifteen which were totally drawn. As expected, Fig. 6a shows that the local stress, monitored at the location of each line, increases while the crack is approaching that line, then attains a maximum when the crack tip is crossing the line. Finally, after the crack has crossed the line, the local stress measured at the location of the line decreases.

Analyzing the diagram of Fig. 6a, the exact time (fatigue cycle) that each line attains a maximum value of stress can be determined. This time corresponds to the fatigue cycle when the crack reaches the reference line. All reference lines were drawn on the thermograph at fixed position in front of the crack-starting notch (Fig 5b). Therefore, knowing the exact positions of reference lines and the fatigue cycle when the crack reaches each reference line, the crack growth rate (da/dN) can be calculated.

The data obtained using lock-in thermography was correlated with crack growth rate values obtained by the conventional compliance method. Fig. 7a depicts the correlation between conventional compliance method and lock-in thermography for crack growth rate determination of aluminum alloy AA7075. It can also be seen, observing the thermographic data, at 80% of total life that an abrupt change of crack growth rate occurs. Therefore, it can be concluded that failure prediction of the specimen's life can be achieved at 80% of its total life. Fig. 7b shows crack growth rates calculated by the conventional compliance method vs. the lock-in thermography method for A359/SiCp composites, as received, T6 heat treated, and HT-1 heat treated, respectively. Examining these figures, one can observe that there is a good correlation between the two methods for determining crack growth rate. Comparison between lock-in thermography and compliance method in

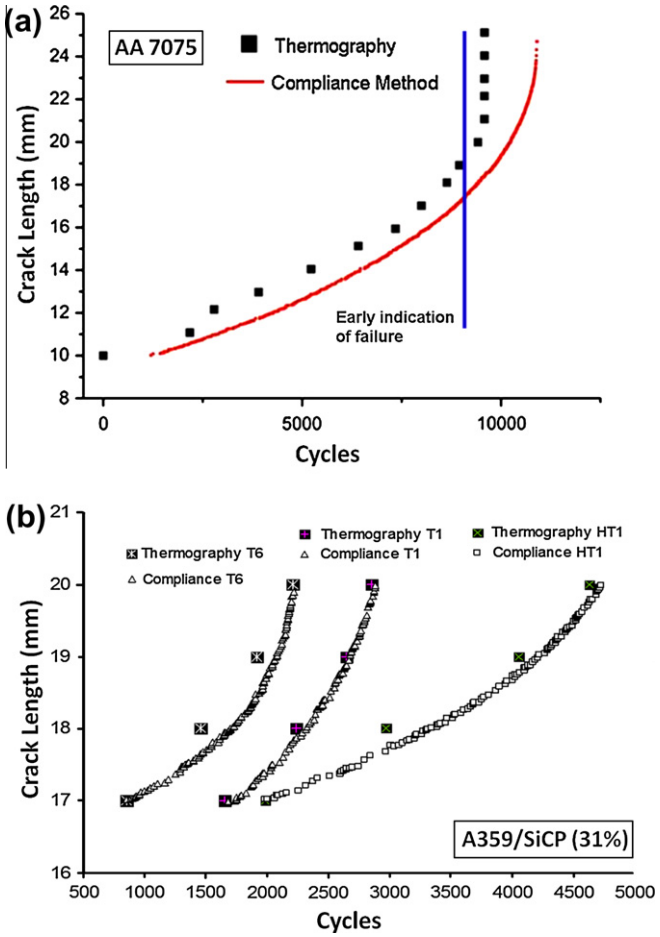

Fig. 7. Crack growth rate determined by the compliance vs. thermography method: (a) for A7075 and (b) for A359/SiCP composite in as received (T1), T6 and HT1 heat treatments.

AA7075 aluminum alloys shows that IR thermography can indicate catastrophic failure approximately 1000 cycles earlier than compliance, demonstrating that thermographic assessment is in effect more accurate than conventional compliance measurement. These

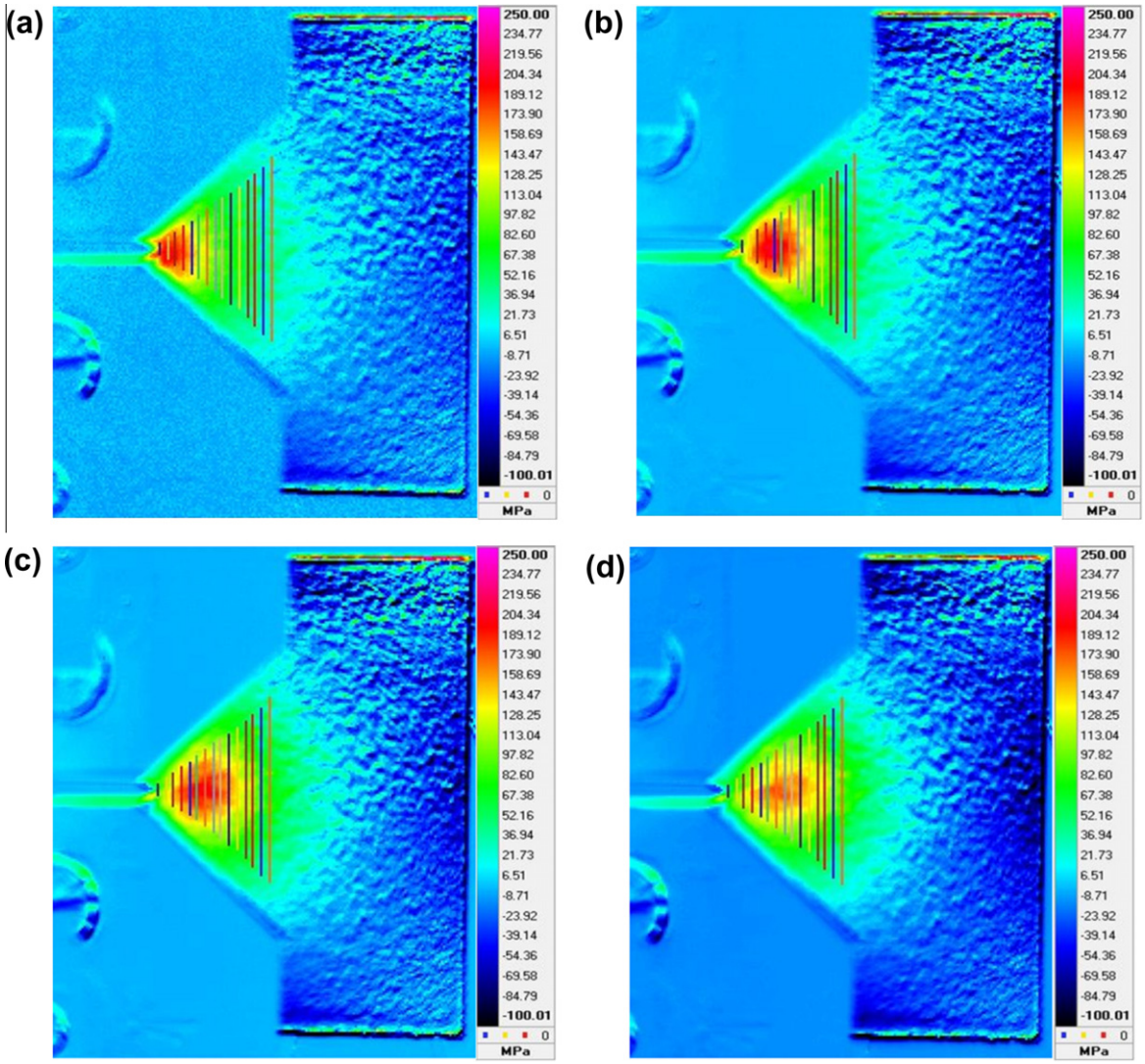

Fig. 8. Progress of stress field due to crack propagation on a CT specimen at: (a) 2000, (b) 6320, (c) 6420, and (d) 9763 cycles.

results were repeatable for all specimens tested, demonstrating that thermographic assessment is in effect more accurate than the conventional compliance measurement.

Comparing Fig. 7a and b it can be concluded that monolithic aluminum exhibits longer fatigue life that the aluminum composite material. This is expected due to the fact that the inclusion of a brittle phase in the aluminum matrix reduces the ductile behavior of the material, enhances crack propagation and finally shortens its fatigue life. This is additionally supported by the higher crack growth rate which is observed in the SiCp reinforced composite (higher slope of the crack length vs. fatigue cycles curve in Fig. 7b) compared to the monolithic aluminum (Fig. 7a).

The new method, based on lock-in thermography, offers the additional ability to discern the crack propagation path. Fig. 8a–d depict the progress of stress field due to crack propagation in a CT coupon. The thermographs shown in Fig. 8 correspond to 2000, 6320, 6420 and 9763 cycles of fatigue life, respectively. In Fig. 8a the stress field indicated with red color is located between the first and the third reference line. At 6320 fatigue cycles (see Fig. 8b), the stress field has been moved and it is detected between the forth and the seventh reference line. After the following 100 cycles (see Fig. 8c) this field was moved rapidly. In Fig. 8d can be observed that the color of this field is not as red as it was in the previous conditions. This can be attributed to the fact that the crack has been increased critically leading to the decrease of max stresses.

5. Acoustic emission results

5.1. Monotonic tensile test

The common procedure for K_{IC} determination includes fatigue of the specimen up to a crack length of 20 mm and consequently monotonic tension up to failure. Therefore, first results of AE monitoring during this monotonic tensile test will be presented. Fig. 9a shows a typical cumulative AE activity graph. Activity starts at around 35 s after load application while the load is approximately at 80% of the maximum. The rate of the incoming AE activity can be considered constant, without strong fluctuations throughout the experiment duration. However, the qualitative features show certain trends as damage is being accumulated. Fig. 9b shows the energy of the AE hits for the duration of the experiment. While the energy is limited to very low values for most of the experiment duration, several seconds before the final failure, some hits with very high intensity are recorded. Similarly, the rise time of the

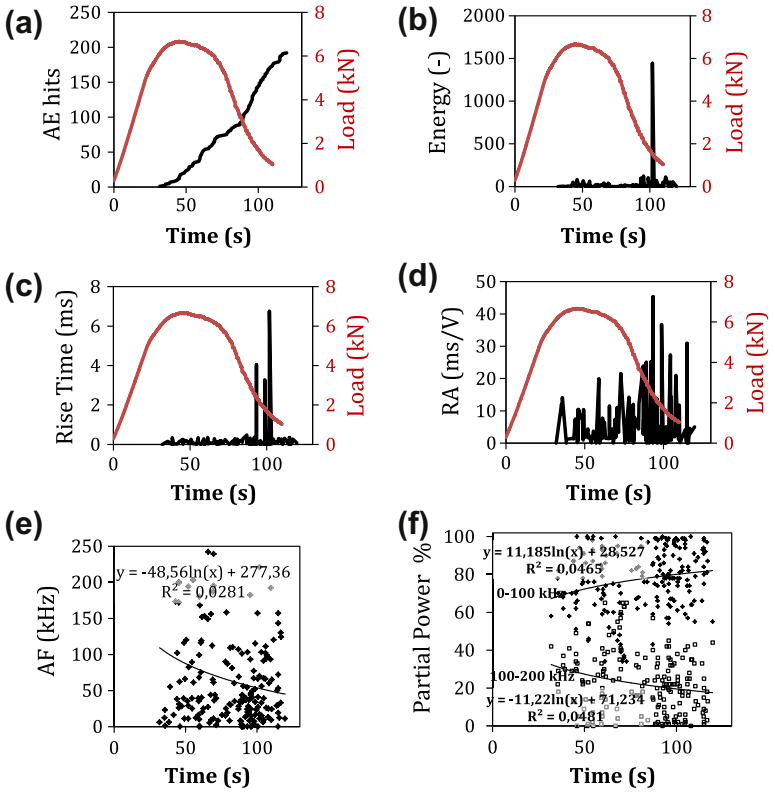

Fig. 9. Time history of: (a) AE cumulative activity, (b) AE energy, (c) rise time, (d) RA value, (e) average frequency, and (f) partial power of different frequency bands.

AE signals at the early stage of loading is relatively low (below 1 ms/V), but as final failure is approaching, several hits with higher rise time are recorded, see Fig. 9c. Consequently, the RA value which is defined by the ratio of rise time to amplitude of the waveform, as explained earlier, exhibits similar trends. At the early stage of loading RA values are limited below 20 ms/V (Fig. 9d). Gradually some hits with higher RA are recorded and at approximately 90 s, when the load has dropped due to ultimate failure, RA values of approximately 40 ms/V are exhibited.

Concerning the frequency content of the AE waves moderate trends can be observed. Fig. 9e shows the AF of the AE hits throughout the experiment. The population of points is quite dispersed in the spectrum and the scatter of the data points is arguably large. However, this is inevitable for a population of several hundreds of signals, (or several thousands) as typically recorded in AE tests. Therefore, the treatment is mainly statistical. Conclusions are not based on any single specific point but on the trends with relation to the loading and fracture conditions. The logarithmic trend line shows a shift of the typical value from approximately 110 kHz at initial low load to 50 kHz at the moment of final failure. As seen from Fig. 9e, the major frequency content of the signals is below 200 kHz. Separating this part of the spectrum in two equal parts (0–100 kHz and 100–200 kHz) it is possible to measure the contribution of each band in the total content of any specific signal. Since the energy is within 0–200 kHz, the sum of the contributions of the two bands will be equal (or almost equal) to unity. The contribution of each of these bands is seen in Fig. 9f as a function of loading time. The content of the lower band (0–100 kHz) increases its contribution from an average of approximately 65–80% as loading continues, while the contribution of the high band (100 kHz to 200 kHz) decreases from 35% to 20% at the same time. This shows that the decreasing trend of AF is due to the relative shift of the content to the lower frequency band. These changes in RA value and AF are related to damage mode shift from tension to shear [18,20–23] as discussed in the next section.

Fig. 10. Typical specimen after failure.

5.2. Fatigue

Fig. 10 shows a half of a typical specimen after the fatigue test to failure. It is stressed out that initially, the crack starts to propagate horizontally as dictated by the notch. After propagation of 5–10 mm though, the cracked surface becomes curved. This is attributed to the maximum diagonal shear stresses that result from the unidirectional tensile external load. Indeed, due to the small thickness of the plate, the stress perpendicular to the surface is zero. Therefore, although the crack starts to propagate horizontally, under the application of the external tensile stress, final fracture occurs due to shear stresses, which are maximum at 45°. This shift in fracture mechanisms (tension to shear) dictates the shift of the emitted AE signature as the experiment continues. Therefore, mounting of AE sensors enables to record not only the cumulative AE activity due to the successive fracture events but also capture the distinct differences of the different modes.

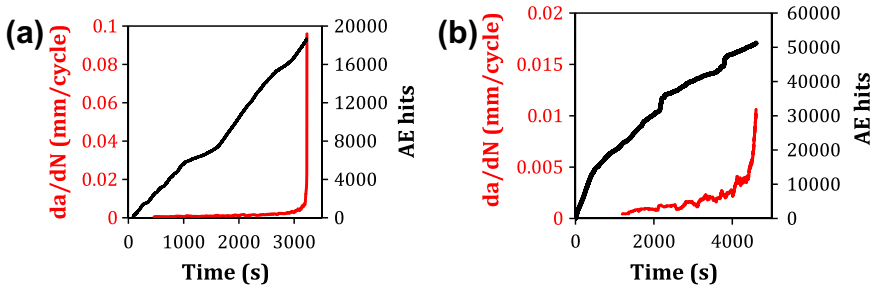

Fig. 11. (a and b) Crack propagation rate and AE cumulative activity for two specimens.

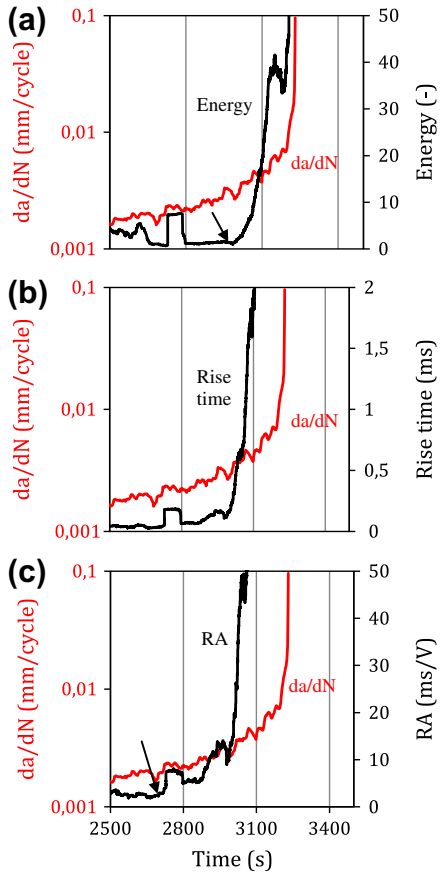

Fig. 12. Crack propagation rate history and (a) energy, (b) rise time, and (c) RA value history during fatigue.

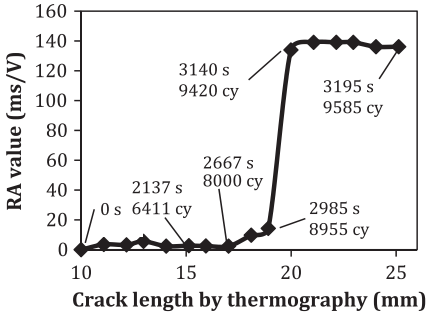

Fig. 13. RA value vs. crack length as measured by LIT.

The cumulative AE activity behavior during fatigue is similar to the one of the monotonic test in the sense that the rate of signals is quite constant, as seen in Fig. 11a. The same figure includes the crack propagation rate (da/dN) throughout the duration of the experiment, which exhibits the expected exponential growth function with time. Final failure occurred at 3231 s. For the specimen of Fig. 11b the trends are quite similar with the exception of the longer duration of the experiment, which led to recording of a larger number of AE hits.

However, as stated earlier, valuable information can be derived by the qualitative parameters of AE, which are directly dependent on the waveform shape. Fig. 12 presents the energy, rise time and RA of the signals as a moving average of the recent 200 hits in order to show the trend more clearly. The figure focuses on the last 15 min of the fatigue life. The AE Energy curve exhibits sharp increase at approximately 3000 s, which is approximately 700 cycles before failure. The point is marked by arrow in Fig. 12a. Specifically, until before 3000 s the energy of a typical hit was close to zero showing low intensity of the crack propagation incidences. As the material proceeded to ultimate failure, energy increased to values of several hundreds. Correspondingly for the rise time although it is initially limited below 0.2 ms, eventually it increases to values higher than 2 ms, as seen in Fig. 12b.

Fig. 12c shows the RA value. It exhibits similar trend near the end of the experiment. Since for the initial part, RA values are limited below 3 ms/V, it is reasonable to assume that these values are connected to the initial tensile mode. Values higher than 10 ms/V exhibited before failure should be connected to shear mode. It should be highlighted that the RA line shows a substantially earlier sign of increase at 2700 s of fatigue (300 s or 900 cycles earlier than energy) as indicated by the arrow of Fig. 12c. This stronger sensitivity may be connected to the dependence of the waveform shape on the dominant fracture mode as discussed in the introduction.

It is interesting to correlate results by the two monitoring methods. The two techniques obtain information from the same fracturing process and the measured indices exhibit a more or less monotonic behavior up to failure. Fig. 13 shows the phenomenological correlation between RA value and the crack length as measured by thermography. While the crack propagates smoothly on a level surface until the length of 15–17 mm (under dominant tensile stresses, as discussed above) RA remains in relatively low values of up to 3 ms/V. After approximately 17 mm of crack length, RA shows increasing trend to 15 ms/V, while as the crack surface becomes curved and the crack propagation rate increases RA exhibits a jump to 140 ms/V. Thereafter it remains at that high level under the predominant shearing action until the end of the experiment.

It is again stressed that the specific AE values hold for the exact experimental conditions, which include the sensor type, sensor separation distance, and specimen geometry. Still, since this is a thin plate specimen, the effect of dispersion is already included on the waveforms even though the waves did not propagate more

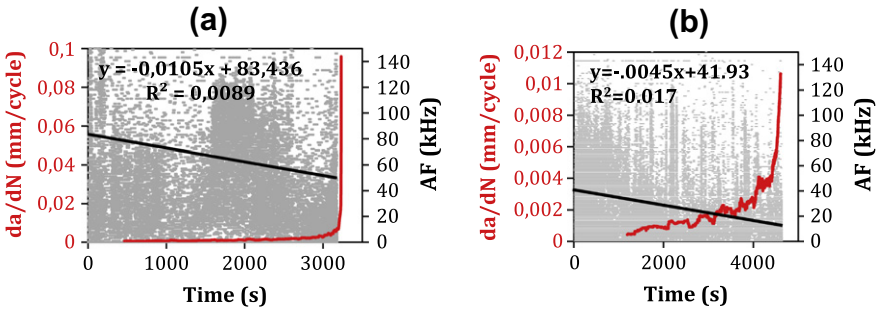

Fig. 14. Crack propagation rate history and average frequency for two specimens.

than a few cm from the crack to the sensors. This effect would be tremendous for larger geometries.

The frequency content of the signals exhibits decreasing trends but in a much smoother way. Fig. 14a shows the AF of all hits. The number of AE hits is much larger for fatigue than for the monotonic tests. Since it is difficult to process the information of a scattered "cloud" of points, the straight fitting curve is included to indicate the trend. Indeed, there is quite a strong shift from an average value of 83 kHz to approximately 50 kHz. The behavior of another specimen is seen in Fig. 14b. The range of values and the trend is similar but the trend line is translated to somehow lower values. In both cases however, the final typical frequency of AE is half of the initial, implying again the reason is the shift from tension to shear. The AF decreasing trend seems moderate compared to the strong increase of other parameters like the RA; however, it is reasonable that different parameters possess different characterization power relatively to the fracture processes. Even though in this case, AF cannot be used as a stand-alone feature for accurate correlations with the crack length or propagation rate, still it is indicative that as damage is being accumulated and the dominant mode shifts from tension to shear, the average frequency content of the signals decrease to the half of the initial.

The above results highlight the capacity of AE to characterize fracture mode, as well as to predict final failure due to fatigue. For controlled experimental conditions (specimen geometry, sensor types and location position, fatigue parameters) when AE parameters (e.g. RA or energy) exhibit a sharp increase this would indicate a remaining life of approximately 1000–1500 cycles. This trend is consistent for the specimens of this study. However, it is necessary to examine its validity in other materials, specimen geometries and loading conditions. This will enable drawing of conclusions regarding the potential of prediction of ultimate failure of metal materials and structures under dynamic loading. Concerning the application of AE, it is emphasized that this is a preliminary study. Different parameters of the AE monitoring should be further examined. In fact the number of AE signals during fatigue is too large for adequate data handling. The application of proper filters in post processing would possibly help to more precisely define the AE trends. Additionally, especially at the last stages of fatigue where the rate of emissions is high it is likely that different emissions overlap and are recorded as one. This possibly contributes to the measurement of signals with longer duration and rise time than in the early stages. However, still this feature nonetheless effectively indicates the switch of the fracture mode.

6. Conclusion

This research is concerned with the study of fracture behavior of aluminum alloys and silicon carbide particle-reinforced (SiC_p) A359 aluminum alloy matrix composites, monitored concurrently by lock-in thermography and acoustic emission.

It was demonstrated that crack growth rate can be effectively monitored by the means of lock-in thermography. The results obtained using the noncontact technique were in agreement with the conventional compliance method. Thermographic monitoring is an accurate method for crack growth assessment even in cases when cracking is not visible on the specimen's surface and propagates inside the material. In addition, it can be concluded that the new method, based on IR thermography, enables early prediction of upcoming catastrophic failure of the specimen at about 80% of its total fatigue life. Moreover, IR lock-in thermography has a significant advantage since it can be used in situations wherein the conventional compliance method cannot be applied.

This study also presents preliminary results on acoustic emission monitoring during tensile and fatigue loading of aluminum coupons. The objective here is to correlate AE parameters that are non-intrusively measured with damage propagation and the dominant fracture mode. Several AE parameters exhibit clear shifts much earlier than final fracture. Specifically, among others, the energy, rise time and the RA value of the AE waveforms strongly increase earlier than 1000 cycles before final failure. This shift of AE indices is attributed to the shift between the dominant modes of fracture; the initial tensile and the ultimate shear which typically occur in thin metal coupons with a notch. This is confirmed by visual observation of the crack's surface after fracture. The exact connection between the fracture mode and the AE signature may still need refinement, but in general it can be concluded that AE parameters are influenced by the damage process (crack propagation rate and mode) and should be studied more in order to lead to warning against final failure and evaluation of the damage stage at any fraction of the materials life.

References

[1] Myriounis DP, Hasan ST, Matikas TE. Microdeformation behaviour of Al–SiC metal matrix composites. Compos Interfaces 2008;15(5):495–514.
[2] Bates D, Smith G, Lu D, Hewitt J. Rapid thermal non-destructive testing of aircraft components. Composites Part B 2000;31(3):175–85.
[3] Nino GF, Ahmed TJ, Bersee HEN, Beukers A. Thermal NDI of resistance welded composite structures. Composites Part B 2009;40(3):237–48.
[4] Wong BS, Tui CG, Bai W, Tan PH, Low BS, Tan KS. Thermographic evaluation of defects in composite materials. Insight: Non-Destr Test Cond Monitor 1999;41(8):504–9.
[5] Brémond P, Potet P. Lock-in thermography. In: Rozlosnik AE, Dinwiddie RB, editors. A tool to analyse and locate thermo-mechanical mechanisms in materials and structures. FL: Orlando; 2001. p. 560–6.
[6] Choi M-Y, Park J-H, Kang K-S, Kim W-T. Application of thermography to analysis of thermal stress in the NDT for compact tensile specimen. In: Proc 12th PCNDT 2006; 2006.
[7] Kim W-T, Choi M-Y, Huh Y-H, Eom S-J. Measurement of thermal stress and prediction of fatigue for STS using Lock-in thermography. In: Proc 12th PCNDT 2006; 2006.
[8] Minh Phong L. Fatigue limit evaluation of metals using an infrared thermographic technique. Mech Mater 1998;28(1–4):155–63.
[9] Krapez JC, Pacou D, Gardette G. Lock-in thermography and fatigue limit of metals. In: Proc QIRT'2000; 2000. p. 277–82.

[10] La Rosa G, Risitano A. Thermographic methodology for rapid determination of the fatigue limit of materials and mechanical components. Int J Fatigue 2000;22(1):65–73.
[11] Yang B, Liaw PK, Wang G, Peter WH, Buchanan RA, Yokoyama Y, et al. Thermal-imaging technologies for detecting damage during high-cycle fatigue. Metall Mater Trans A 2004;35(A1):15–23.
[12] Plekhov O, Palin-Luc T, Saintier N, Uvarov S, Naimark O. Fatigue crack initiation and growth in a 35CrMo4 steel investigated by infrared thermography. Fatigue Fract Eng Mater Struct 2005;28(1–2):169–78.
[13] Ait Aouit D, Ouahabi A. Monitoring crack growth using thermography. Suivi de fissuration de matériaux par thermographie 2008;336(8):677–83.
[14] Kordatos, E.Z., Matikas, T.E. Developing damage metrics for metallic structures undergoing fatigue using real-time thermographic evaluation, Proc. SPIE 7982, 79820U (2011). doi:10.1117/12.881019.
[15] Risitano A, Risitano G. Cumulative damage evaluation of steel using infrared thermography. Theor Appl Fract Mech 2010;54(2):82–90.
[16] Kaiser J. Results and conclusions from measurements of sound in metallic materials under tensile stress: technische hochshule Munich; 1950.
[17] Grosse CU, Ohtsu M. Acoustic emission testing. Heidelberg: Springer; 2008.
[18] Aggelis DG, Shiotani T, Momoki S, Hirama A. Acoustic emission and ultrasound for damage characterization of concrete elements. ACI Mater J 2009;106(6):509–14.
[19] Hensman J, Pullin R, Eaton M, Worden K, Holford KM, Evans SL. Detecting and identifying artificial acoustic emission signals in an industrial fatigue environment. Meas Sci Technol 2009;20(4).
[20] Committee RT. Recommendation of RILEM TC 212-ACD: acoustic emission and related NDE techniques for crack detection and damage evaluation in concrete*. Mater Struct 2010;43(9):1187–9.
[21] Ohtsu M, Tomoda Y. Phenomenological model of corrosion process in reinforced concrete identified by acoustic emission. ACI Mater J 2008;105(2):194–9.
[22] Aggelis DG, Soulioti DV, Sapouridis N, Barkoula NM, Paipetis AS, Matikas TE. Acoustic emission characterization of the fracture process in fibre reinforced concrete. Constr Build Mater 2011;25(11):4126–31.
[23] Aggelis DG, Barkoula NM, Matikas TE, Paipetis AS. Acoustic emission monitoring of degradation of cross ply laminates. J Acoust Soc Am 2010;127(6):EL246.
[24] Anastassopoulos AA, Philippidis TP. Clustering methodology for the evaluation of acoustic emission from composites. NDT and E Int 1997;30(2):108. -.
[25] Soulioti D, Barkoula NM, Paipetis A, Matikas TE, Shiotani T, Aggelis DG. Acoustic emission behavior of steel fibre reinforced concrete under bending. Constr Build Mater 2009;23(12):3532–6.
[26] Brown J, Vendra L, Rabiei A. Bending properties of Al-steel and steel–steel composite metal foams. Metall Mater Trans A 2010;41(11):2784–93.
[27] Quispitupa A, Shafiq B, Just F, Serrano D. Acoustic emission based tensile characteristics of sandwich composites. Compos Part B: Eng 2004;35(6-8):563–71.
[28] Naderi M, Kahirdeh A, Khonsari MM. Dissipated thermal energy and damage evolution of Glass/Epoxy using infrared thermography and acoustic emission. Composites Part B 2012; 43(3):1613-1620.
[29] Majumdar BS, Matikas TE, Miracle DB. Experiments and analysis of fiber fragmentation in single and multiple-fiber SiC/Ti-6Al-4V metal matrix composites. Composites Part B 1998;29(2):131–45.
[30] Rousset G, Martin E, Lamon J. In situ fibre strength determination in metal matrix composites. Compos Sci Technol 2009;69(15–16):2580–6.
[31] Roberts TM, Talebzadeh M. Acoustic emission monitoring of fatigue crack propagation. J Constr Steel Res 2003;59(6):695–712.
[32] Boinet M, Bernard J, Chatenet M, Dalard F, Maximovitch S. Understanding aluminum behaviour in aqueous alkaline solution using coupled techniques: Part II: acoustic emission study. Electrochim Acta 2010;55(10):3454–63.
[33] Clough RB, McDonough WG. The measurement of fiber strength parameters in fragmentation tests by using acoustic emission. Compos Sci Technol 1996;56(10):1119–27.
[34] Aggelis DG, Kordatos EZ, Matikas TE. Acoustic emission for fatigue damage characterization in metal plates. Mech Res Commun 2011;38(2):106–10.
[35] Thomson W. On the dynamical theory of heat. Trans Roy Soc Edin 1853;20:261–83.
[36] Bremond P. New developments in thermoelastic stress analysis by infrared thermograph. IV Conferencia Panamericana de END; 2007.
[37] Maldague XPV. Introduction to NDT by active infrared thermography. Mater Eval 2002;60(9):1060–73.
[38] Kordatos, E.Z., Myriounis, D.P., Hasan, S.T., Matikas, T.E. Monitoring the fracture behavior of SiCp/Al alloy composites using infrared lock-in thermography. Proc. SPIE 7294, 72940X (2009). doi:10.1117/12.815207.
[39] Myriounis DP, Kordatos EZ, Hasan ST, Matikas TE. Crack-tip stress field and fatigue crack growth monitoring using infrared lock-in thermography in A359/SiCp composites. Strain 2011;47:e619–27.